Ternary Nanocomposites of Porphyrin, Angular Au Nanoparticles and Reduced Graphene Oxide: Photocatalytic Synthesis and Enhanced Photocurrent Generation

ARTICLE *in* CHEMCATCHEM · AUGUST 2012

Impact Factor: 4.56 · DOI: 10.1002/cctc.201200128

DOI: 10.1002/cctc.201200128

Ternary Nanocomposites of Porphyrin, Angular Au Nanoparticles and Reduced Graphene Oxide: Photocatalytic Synthesis and Enhanced Photocurrent Generation

Haiyan Li,[a] Sen Liu,[a] Jingqi Tian,[a, b] Lei Wang,[a] Wenbo Lu,[a] Yonglan Luo,[a] Abdullah M. Asiri,[c, d] Abdulrahman O. Al-Youbi,[c, d] and Xuping Sun*[a, c, d]

In recent years, graphene has attracted intense interest from both academic and industrial communities, owing to its unique properties including high mobility of charge carriers, thermal conductivity, mechanical strength, and specific surface areas, as well as its great potential in a variety of applications, such as electronic devices, batteries, solar energy conversion, and catalysis etc.[1] The first challenge is to process graphene sheets for their use in practical applications.[2] Till now, although many methods have been developed to fabricate graphene materials, including micromechanical exfoliation, chemical vapor deposition, and reduction of graphene oxide (GO) etc.,[1a,3] the chemical reduction of GO is the most common route to low-cost, large-scale production of reduced GO (RGO).[3d,4] However, the reducing agents used, such as hydrazine, dimethylhydrazine, and sodium borohydride, are either toxic or hazardous[3b,5] and pose environmental and health risks. Thus, the development of environmentally-friendly preparative strategy is highly desired.

On the other hand, extensive research has focused on constructing graphene-based nanocomposites because the composites not only combine the merits of each component, but offer the potential to introduce new properties that can potentially be used in a diverse range of applications.[6] Indeed, considerable effort has been devoted to fabricating binary composites of graphene as a two-dimensional (2D) scaffold and metal nanoparticles, semiconductor nanoparticles, or photoactive molecules as a viable alternate to boost the efficiency of various catalytic and storage reactions in energy conversion applications.[7] To the best of our knowledge, however, very little attention has been paid to graphene-based organic–inorganic ternary composites. Only recently have Kamat and co-workers developed composites of Zn-porphyrin, ZnO nanoparticles, RGO to mimic photoinduced sequential multistep electron transfer (ET) in photosynthesis.[8] Although this hierarchical ET cascade system exhibits high photocurrent generation, it suffers in that the visible light can only be absorbed by the porphyrin component.

In this communication, we demonstrate a green photocatalytic strategy toward RGO with the use of Sn-porphyrin (SnP) as an effective photocatalyst for the reduction of GO under visible-light irradiation. Subsequently, SnP-catalyzed photoreduction of Au^{III} on the binary composites leads to organic–inorganic ternary nanocomposites of SnP, angular Au nanoparticles (AuNPs). and RGO. The AuNPs loading on RGO can be facilely tuned by the irradiation time. Most importantly, both SnP and AuNPs serve as photoactive, visible-light-absorbing components and the synergistic effect of surface plasmon resonance excitation in the AuNPs and SnP yields a 27-fold increase in the photocurrent when illuminated at $\lambda = 550$ nm.

Shown in Figure 1a are the UV/vis absorption spectra of aqueous dispersions of GO, SnP, SnP/GO, and SnP/RGO. GO exhibits a strong peak centered at $\lambda \approx 235$ nm and a shoulder peak at $\lambda \approx 300$ nm corresponding to π–π^* transitions of aromatic C=C band and n–π^* transitions of C=O band, respectively. In the absence of RGO, SnP shows a Soret band at $\lambda \approx 402$ nm and two less intense Q-bands between $\lambda = 500$–650 nm, which are attributed to π–π^* excitation of the porphyrin ring.[9] In the presence of GO, maximum of the Soret band of SnP red-shifts from $\lambda = 402$ to 409 nm, which can be attributed to the adsorption of SnP molecule on GO driven by π–π stacking interactions between the porphyrin moiety and the GO.[10] After visible-light irradiation, the peak at $\lambda = 235$ nm red-shifts to $\lambda = 261$ nm, the shoulder peak at $\lambda = 300$ nm disappears, and the absorbance in the whole spectral region increases, indicating the restoration of the π-conjugation network within the graphene sheet.[11] Shown in Figure 1b are the Raman spectra of GO and SnP/RGO. GO exhibits two characteristic bands: the D band at $\nu \approx 1351$ cm^{-1}, arising from a breathing mode of κ-point photons of A_{1g} symmetry, which is attributed to local defects and disorders; the G band at $\nu \approx 1597$ cm^{-1}, arising from the first order scattering of the E_{2g} phonon of sp^2 C atoms.[6] The Raman spectrum of SnP/RGO also contains both D and G bands (at $\nu \approx 1351$ and 1601 cm^{-1}, respectively), the increase of G band in the frequency should be attributed to the interaction with SnP molecules and RGO.[12] The obtained values of the I_D/I_G ratio are 0.82 and 0.97

[a] Dr. H. Li, Dr. S. Liu, J. Tian, L. Wang, W. Lu, Y. Luo, Prof. X. Sun
State Key Lab of Electroanalytical Chemistry
Changchun Institute of Applied Chemistry
Chinese Academy of Sciences
Changchun 130022 (China)
Fax: (+86) 431-85262065
E-mail: sunxp@ciac.jl.cn

[b] J. Tian
Graduate School of the Chinese Academy of Sciences
Beijing 100039 (China)

[c] Prof. A. M. Asiri, A. O. Al-Youbi, Prof. X. Sun
Chemistry Department, Faculty of Science
King Abdulaziz University
Jeddah 21589 (Saudi Arabia)

[d] Prof. A. M. Asiri, A. O. Al-Youbi, Prof. X. Sun
Center of Excellence for Advanced Materials Research
King Abdulaziz University
Jeddah 21589 (Saudi Arabia)

Supporting information for this article is available on the WWW under http://dx.doi.org/10.1002/cctc.201200128.

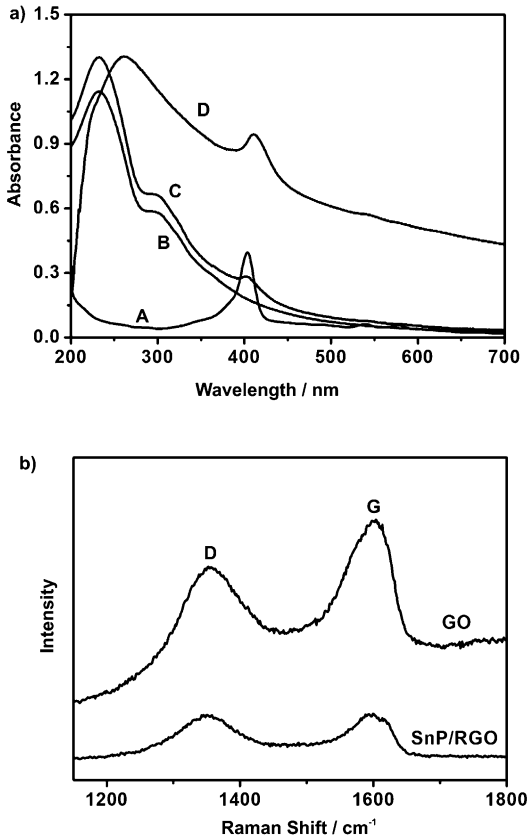

Figure 1. a) UV/vis absorption spectra of aqueous dispersions of A) SnP, B) GO, C) SnP/GO, and D) SnP/RGO; b) Raman spectra of GO and SnP/RGO.

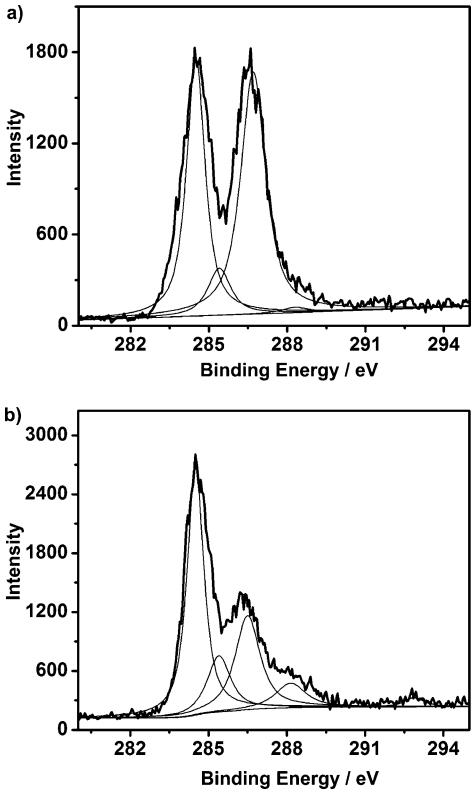

Figure 2. C 1s XPS spectra for a) GO and b) SnP/RGO.

for GO and SnP/RGO, respectively, providing another piece of evidence to support the reduction of GO after the irradiation.[13]

Shown in Figure 2 are the C 1s XPS spectra for GO and SnP/RGO. Analysis of the GO spectra reveals four different types of C 1s peaks at 284.5, 285.4, 286.7, and 288.6 eV, corresponding to C–C, C–OH, C–O (epoxy), and C=O bonds, respectively (Figure 2 a).[14] The peak intensity of C–O in SnP/RGO, however, decreases tremendously, and the content of C–C correspondingly increases dramatically at the same time, as shown in Figure 2 b. These results confirm the reduction of GO. In addition, SnP/RGO also shows a new peak characteristic of C (π–π^*)of aromatic ring at 292.2 eV,[15] indicating the presence of SnP. The observation of increased peak intensity of C=O is attributed to the presence of SnP.

Shown in Figure 3 a is the low magnification TEM image of SnP/AuNPs/RGO nanocomposites after a 15 min irradiation period, indicating that a large amount of nanoparticles are generated on the surface of RGO. The high magnification TEM image shown in Figure 3 b further reveals the nanoparticles are well separated from each other and present angular-shape morphology. The HRTEM image taken from one nanoparticle (inset in Figure 3 b) reveals clear lattice fringes with an interplane distance of 0.236 nm, corresponding to the (111) lattice space of metallic Au. The corresponding EDX spectrum (Figure S1) also confirms the presence of Au element. Importantly, the AuNP loading on RGO can be facilely tuned by the irradia-

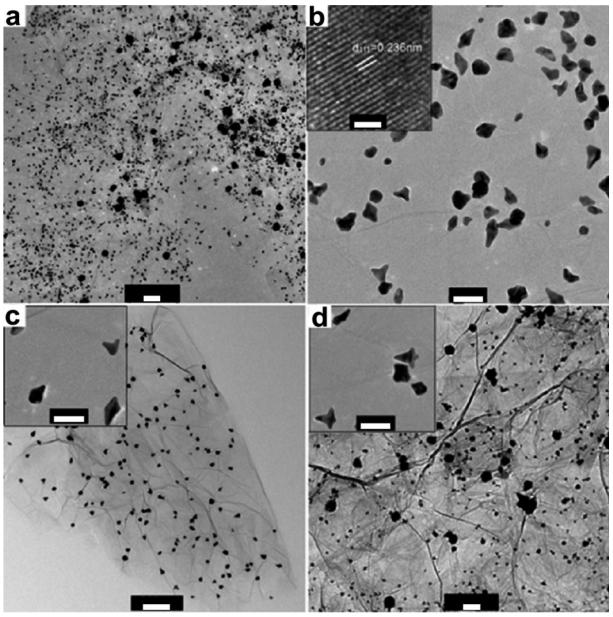

Figure 3. a) Low and b) high magnification TEM images of SnP/AuNPs/RGO nanocomposites with irradiation time of 15 min (inset: HRTEM micrograph with the lattice fringes). c) and d) show low magnification TEM images of the ternary nanocomposites with irradiation time of 2 min and 5 min, respectively (inset: high magnification TEM image). Scale bars for a, c, d) = 200 nm and for b) = 50 nm. Inset scale bars b) = 1 nm and c, d) = 50 nm.

tion time involved. Shown in Figure 3c and 3d are the TEM images of the products obtained with irradiation time of 2 min and 5 min, respectively, suggesting increased irradiation time leads to an increased loading of AuNPs. Also note that only near spherical AuNPs were obtained in the absence of RGO under otherwise identical experimental conditions (Figure S2), indicating the roles of RGO as a medium to tune the growth behaviors of Au nanocrystals.

We also collected time-dependent extinction spectra of the aqueous dispersion of SnP/AuNPs/RGO nanocomposites, as shown in Figure S3. Before irradiation, no plasmon absorption band characteristic of AuNPs is observed (curve a). After a 2 min irradiation, a band at $\lambda = 567$ nm is observed (curve b), indicating the formation of AuNPs. With increased irradiation time, we observe an increase of the plasmon absorption band in intensity (curve c and d), which can be attributed to an increase of the amount of reduced Au. These results are quite consistent with above TEM observations.

Shown in Figure 4 are the transient photocurrent graphs of anodic RGO, SnP/RGO, AuNPs/RGO, and SnP/AuNPs/RGO nanocomposites irradiated with different wavelengths for 20 s ($\lambda =$ 520 nm, 258 mW cm^{-2}; $\lambda = 550$ nm, 190 mW cm^{-2}). To compare the photocurrent response, the pure RGO and AuNPs/RGO nanocomposites (Figure S4) were prepared by chemical reduction method. As can be seen, the pure RGO show no photocurrent response under both $\lambda = 520$ and 550 nm illumination. A small anodic photocurrent is obtained for SnP/RGO (0.094 μA) and AuNPs/RGO nanocomposites (0.095 μA) under $\lambda = 520$ nm illumination, which means the photogenerated electrons move to the bulk and subsequently transfer to the ITO electrode, leaving holes on the outer surface. However, compared with the binary SnP/RGO nanocomposites, a 2.6-fold enhancement in the photocurrent is observed for ternary SnP/AuNPs/RGO nanocomposites, indicating that the enhanced photocurrent response can be attributed to a synergistic effect of the surface plasmon resonance excitation in the AuNPs[16] and SnP. When the irradiation wavelength is $\lambda = 550$ nm, which is much closer to the plasmon absorption band of AuNPs ($\lambda = 567$ nm), a photocurrent is obtained for SnP/RGO (0.035 μA) and AuNPs/RGO nanocomposites (0.12 μA), and the SnP/AuNPs/RGO nanocomposites exhibit a 27-fold increase in the photocurrent compared with the binary SnP/RGO nanocomposites, which should be attributed to more effective plasmon resonance in the AuNPs under $\lambda = 550$ nm illumination.

For SnP/RGO nanocomposites, SnP can be excited easily under the visible light, then the photogenerated electrons inject from $SnP^{-\bullet}$ (−0.66 V vs. NHE) to RGO sheets.[17] The 2D graphene sheets have excellent capability to accept and shuttle electrons,[6e] leading to photocurrent generation. In contrast, for AuNPs/RGO, SnP/AuNPs/RGO nanocomposites, because Au (0.45 V vs. NHE)[18] and RGO sheets have different Fermi levels, charge must be transferred between them to equilibrate their Fermi levels when they contact with each other. The direct electrons transfer from plasmonic AuNPs and $SnP^{-\bullet}$ to RGO sheets can take place for SnP/AuNPs/RGO nanocomposites, simultaneously. Moreover, the electrons injection from $SnP^{-\bullet}$ into the Fermi level of Au is thermodynamically favorable, providing an additional photocurrent generation pathway, which may be the reason for enhanced photocurrent. Then the collected electrons transfer to the ITO electrode from the RGO network, the oxidized porphyrin ($SnP^{+\bullet}$) and holes generated in the AuNPs undergo reduction with EDTA in the electrolyte solution, resulting in a greatly enhanced anodic photocurrent. Shown in Scheme 1 is a diagram that illustrates the photogenerated charge transport in ternary SnP/AuNPs/RGO nanocomposites.

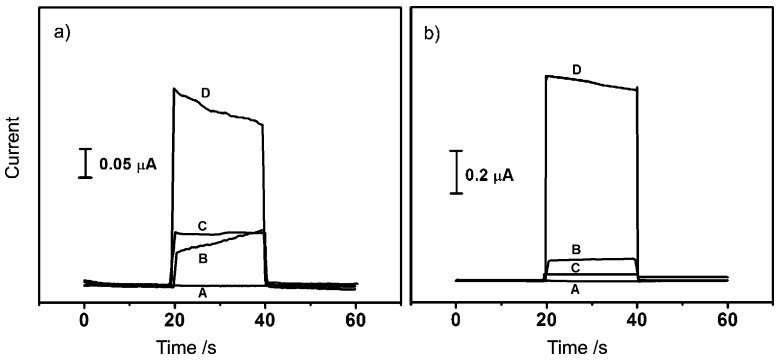

Figure 4. Transient photocurrent of anodic A) RGO, B) AuNPs/RGO, C) SnP/RGO and D) SnP/AuNPs/RGO nanocomposites irradiated with wavelength a) $\lambda = 520$ nm and b) $\lambda = 550$ nm for 20 s under an electrode potential of 0 V versus Ag/AgCl.

In summary, organic–inorganic ternary SnP/angular AuNPs/RGO nanocomposites have been prepared successfully for the first time by a green photocatalytic

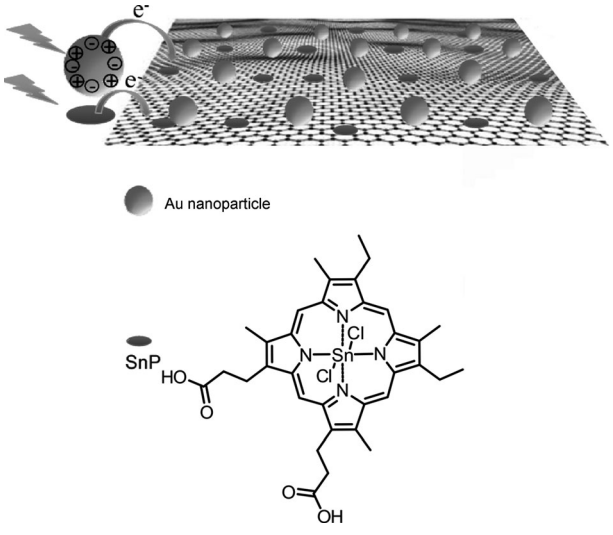

Scheme 1. Schematic diagram illustrating the photogenerated charge transport in ternary SnP/AuNPs/RGO nanocomposites.

strategy with the use of SnP as an effective photocatalyst for the reduction of both GO and Au^{III} under visible-light irradiation. The RGO sheets play a critical role in controlling the morphology of Au nanocrystals, and the AuNPs loading can be tuned by irradiation time. The significant enhancement in photocurrent is attributed to the synergistic effect of surface plasmon resonance excitation in the AuNPs and SnP. Our present study is important for the following two reasons: 1) It is the first demonstration that uses porphyrin as a photocatalyst for green synthesis of RGO; 2) It provides a general methodology for constructing multicomponent graphene-based nanohybrids for energy and other applications.

Experimental Section

Reagents

8,13-Bis(vinyl)-3,7,12,17-tetramethyl-21 H,23H-porphine-2,18-dipropionic acid tin(IV) dichloride (SnP) (99.95%) was purchased from Frontier Scientific, Inc. (Logan, UT, USA). Solutions of SnP in ethanol was prepared as stock solutions in advance, and kept in a refrigerator in a light protected foiled vial. Graphite powder and $HAuCl_4$ were from Aladin Ltd. (Shanghai, China). Unless otherwise specified, the other reagents and materials involved were obtained commercially from the Beijing Chemical Reagent Plant (Beijing, China) and used as received without further purification. The water used throughout all experiments was purified through a Millipore system, and the experiments were performed at room temperature and humidity.

Preparation of GO

GO was prepared from natural graphite powder through a modified Hummers' method. In a typical synthesis, graphite (1 g) was added into 98% H_2SO_4 (23 mL), kept stirring at room temperature for 24 h then, $NaNO_3$ (100 mg) was introduced into the mixture and stirred for 30 min. Subsequently, the mixture was kept below 5 °C by ice bath, and $KMnO_4$ (3 g) was slowly added into the mixture. After being heated to 35–40 °C, the mixture was stirred for another 30 min. After that, water (46 mL) was added into above mixture during a period of 25 min. Finally, water (140 mL) and 30% H_2O_2 (10 mL) were added into the mixture to stop the reaction. After the unexploited graphite in the resulting mixture was removed by centrifugation, the as-synthesized GO was dispersed into individual sheets in distilled water at a concentration of 0.5 mg mL^{-1} with the aid of ultrasound for further use.

Preparation of ternary SnP/AuNPs/RGO nanocomposites

In a typical synthesis, reagents were GO (1 mL of 0.5 mg mL^{-1} in deionized water); SnP (40 μL of 200 μM in ethanol), and triethanolamine (6 mL of 45 mM TEA in deionized water). All the reagents were added to a glass reactor, cooling water was circulated outside the reactor to maintain the reaction temperature at 25 °C, then irradiated with a 500 W xenon lamp (CHFXQ500W, Beijing) with a UV cutter filter ($\lambda > 400$ nm) for 15 min under magnetic stirring. After that, $HAuCl_4$ (100 μL of 24.3 mM in deionized water) was added to the above solution, and then irradiated at the same condition. At the given time intervals, the reaction products were taken from the solution. The products were harvested by centrifugation, followed by washing with water three times to remove residual TEA and SnP from the surface of the RGO.

Characterization and measurements

UV/vis absorption spectra were recorded by using a UV5800 spectrophotometer. Raman spectra were obtained by using J-Y T64000 Raman spectrometer with $\lambda = 514.5$ nm wavelength incident laser light. X-ray photoelectron spectroscopy (XPS) analysis was measured by using an ESCALABMK II X-ray photoelectron spectrometer using Mg as the exciting source. Transmission electron microscopy (TEM) measurements were made by using a HITACHI H-8100 EM (Hitachi, Tokyo, Japan) with an accelerating applied potential of 200 kV. The sample for TEM characterization was prepared by placing a drop of the dispersion on carbon-coated copper grid and dried at room temperature. Photoelectrochemical measurements were composed by using a CHI 660D electrochemical analyzer (CH Instruments, Inc., Shanghai), a 500 W xenon lamp (CHFXQ500W, Beijing) with an appropriate band-pass filter (full width at half maximum (fwhm) = 15 nm), $\lambda = 520$ nm, 550 nm), and a homemade three-electrode cell using a KCl-saturated Ag/AgCl electrode, a platinum wire, and RGO/SnP nanohybrids with or without Au as the reference, counter, and working electrodes, respectively. RGO/SnP/Au electrodes were prepared by depositing suspensions made of RGO/SnP/Au and absolute ethanol onto indium-tin oxide glass (ITO). The supporting electrolyte was 1 M Na_2SO_4, and 5 mM EDTA was used as the sacrificial electron donor. The above solution was purged with high-purity nitrogen for at least 15 min prior to experiments.

Acknowledgements

This work was supported by the National Natural Science Foundation of China (No. 21175129), the National Basic Research Program of China (No. 2011CB935800), and the Scientific and Technological Development Plan Project of Jilin Province (Nos. 20100534 and 20110448).

Keywords: gold · graphene · photocatalytic · nanoparticles · surface plasmon resonance

[1] a) K. S. Novoselov, A. K. Geim, S. V. Morozov, D. Jiang, Y. Zhang, S. V. Dubonos, I. V. Girgorieva, A. A. Firsov, *Science* **2004**, *306*, 666–669; b) C. Lee, X. Wei, J. W. Kysar, J. Hone, *Science* **2008**, *321*, 385–388; c) A. K. Geim, *Science* **2009**, *324*, 1530–1534; d) C. N. R. Rao, A. K. Sood, K. S. Subrahmanyam, A. Govindaraj, *Angew. Chem.* **2009**, *121*, 7890–7916; *Angew. Chem. Int. Ed.* **2009**, *48*, 7752–7777; e) W. Yang, K. R. Ratinac, S. P. Ringer, P. Thordarson, J. J. Gooding, F. Braet, *Angew. Chem.* **2010**, *122*, 2160–2185; *Angew. Chem. Int. Ed.* **2010**, *49*, 2114–2138; f) M. J. Allen, V. C. Tung, R. B. Kaner, *Chem. Rev.* **2010**, *110*, 132–145; g) X. Huang, X. Qi, F. Boey, H. Zhang, *Chem. Soc. Rev.* **2011**, DOI: 10.1039/c1s15078b.

[2] M. Segal, *Nat. Nanotechnol.* **2009**, *4*, 612–614.

[3] a) P. W. Sutter, J. I. Flege, E. A. Sutter, *Nat. Nanotechnol.* **2008**, *3*, 406–411; b) D. Li, M. B. Muller, S. Gilje, R. B. Kaner, G. G. Wallace, *Nat. Nanotechnol.* **2008**, *3*, 101–105; c) V. C. Tung, M. J. Allen, Y. Yang, R. B. Kaner, *Nat. Nanotechnol.* **2009**, *4*, 25–29; d) S. Park, R. S. Ruoff, *Nat. Nanotechnol.* **2009**, *4*, 217–224.

[4] D. R. Dreyer, S. Park, C. W. Bielawski, R. S. Ruoff, *Chem. Soc. Rev.* **2010**, *39*, 228–240.

[5] a) S. Stankovich, D. A. Dikin, G. H. B. Dommett, K. M. Kohlhaas, E. J. Zimney, E. A. Stach, R. D. Piner, S. T. Nguyen, R. S. Ruoff, *Nature* **2006**,

442, 282 – 286; b) W. Gao, L. B. Alemany, L. Ci, P. M. Ajayan, *Nat. Chem.* **2009**, *1*, 403 – 408.
[6] a) Y. Xu, L. Zhao, W. Hong, C. Li, G. Shi, *J. Am. Chem. Soc.* **2009**, *131*, 13490 – 13497; b) Y. Wang, Z. Li, D. Hu, C. Lin, J. Li, Y. Lin, *J. Am. Chem. Soc.* **2010**, *132*, 9274 – 9276; c) C. Lu, J. Li, M. Lin, Y. Wang, H. Yang, X. Chen, G. Chen, *Angew. Chem.* **2010**, *122*, 8632 – 8635; *Angew. Chem. Int. Ed.* **2010**, *49*, 8454 – 8457; d) Z. Tang, S. Shen, J. Zhang, X. Wang, *Angew. Chem.* **2010**, *122*, 4707 – 4711; *Angew. Chem. Int. Ed.* **2010**, *49*, 4603 – 4607; e) I. V. Lightcap, T. H. Kosel, P. V. Kamat, *Nano Lett.* **2010**, *10*, 577 – 583.
[7] P. V. Kamat, *J. Phys. Chem. Lett.* **2011**, *2*, 242 – 251.
[8] H. Hayashi, I. V. Lightcap, M. Tsujimoto, M. Takano, T. Umeyama, P. V. Kamat, H. Imahori, *J. Am. Chem. Soc.* **2011**, *133*, 7684 – 7687.
[9] W. Kim, T. Tachikawa, T. Majima, C. H. Li, H. J. Kim, W. Y. Choi, *Energy Environ. Sci.* **2010**, *3*, 1789 – 1795.
[10] A. Wojcik, P. V. Kamat, *ACS Nano* **2010**, *4*, 6697 – 6706.
[11] Y. Guo, S. Guo, J. Ren, Y. Zhai, S. Dong, E. Wang, *ACS Nano* **2010**, *4*, 4001 – 4010.
[12] B. Das, R. Voggu, C. S. Rout, C. N. R. Rao, *Chem. Commun.* **2008**, 5155 – 5157.
[13] S. Stankovich, D. A. Dikin, R. D. Piner, K. A. Kohlhaas, A. Kleinhammes, Y. Y. Jia, Y. Wu, S. T. Nguyen, R. S. Ruoff, *Carbon* **2007**, *45*, 1558 – 1565.
[14] S. Gilje, S. Han, M. Wang, K. L. Wang, R. B. Kaner, *Nano Lett.* **2007**, *7*, 3394 – 3398.
[15] a) Y. Xu, H. Bai, G. Lu, C. Li, G. Shi, *J. Am. Chem. Soc.* **2008**, *130*, 5856 – 5857; b) E. Treossi, M. Melucci, A. Liscio, M. Gazzano, P. Samori, V. Palermo, *J. Am. Chem. Soc.* **2009**, *131*, 15576 – 15577.
[16] Y. Tian, T. Tatsuma, *J. Am. Chem. Soc.* **2005**, *127*, 7632 – 7637.
[17] P. Quaresma, L. Soares, L. Contar, A. Miranda, I. Osório, P. A. Carvalho, R. Franco, E. Pereira, *Green Chem.* **2009**, *11*, 1889 – 1893.
[18] V. Subramanian, E. E. Wolf, P. V. Kamat, *J. Am. Chem. Soc.* **2004**, *126*, 4943 – 4950.

Received: March 1, 2012
Revised: March 17, 2012
Published online on June 4, 2012

